RSC Advances

PAPER

View Article Online
View Journal | View Issue

Cite this: *RSC Adv.*, 2025, **15**, 2651

Cellulose nanocrystal composite films for contactless moisture-electric conversion†

Wenna Ge,[a] Quanmao Wei,[a] Xu Wang,[a] Chenguang Lu,[a] Hu Han*[b] and Yahua Liu *[ac]

Received 30th November 2024
Accepted 15th January 2025

DOI: 10.1039/d4ra08459d

rsc.li/rsc-advances

The ability to convert moisture signals into electrical signals through contactless control underpins a wide range of applications, including health monitoring, disaster warning, and energy harvesting. Despite its potential, the effective utilization of low-grade energy remains challenging, as it often requires complex device architectures that limit scalability and integration, particularly in wearable technologies. Here, we present a soft, flexible moisture-electric converter made from cellulose nanocrystals and polyvinyl alcohol composite films, designed for a novel touchless interactive platform. The device autonomously generates an electric output voltage of 200–700 mV in response to ambient moisture variations without requiring an external energy source. Its design, featuring a soft-adhered conductive carbon strip coupled with the composite film, provides high flexibility and portability. This configuration facilitates the creation of a non-contact control interface that seamlessly interacts with biological moisture from the human body, demonstrated by a mask that detects breathing conditions and a panel that measures contact distance. These advancements offer a promising pathway for developing flexible, intelligent electronic devices for wearable and touchless technologies.

1 Introduction

With the increasing demand for wearable and portable devices, sensors that are capable of lower power consumption, smaller sizes, and high accuracy are highly preferred.[1] A flexible, simple design is essential for wearable sensors.[2,3] Meanwhile, non-invasive sensing eliminates the risks of contamination and damage from physical contact, thereby enhancing the durability of the sensing system. Therefore, non-contact sensing holds significant research value in this field.[4–6] Contactless signal transmission is particularly valuable in areas like hospitals and public spaces, where reducing the risk of cross-infection from bacteria and viruses is critical.[7–10] For instance, such technology can meet the specialized detection needs of burn patients or individuals with infectious diseases. Additionally, contactless sensors have promising applications in human-machine interaction systems, including smart lights, door locks, and home appliances.[7,11,12] In virtual and augmented reality, they enable natural and immersive interactions with virtual environments through gestures and movements.[13] However, widespread adoption of contactless sensors is hindered by high manufacturing costs, complex signal processing, intricate structures, and limitations in use distance and access methods, particularly in self-powered devices.[14–17] Conventional sensing technologies, such as piezoelectric materials that convert mechanical energy into electrical signals,[18–21] and triboelectric generators that harness frictional energy, have been widely adopted in various electronic products.[22–28] However, these approaches predominantly rely on physical contact, and non-contact signal transmission remains an area requiring further exploration.

Recent research has shown that moisture could be recognized as a stimulus by sensors,[29,30] which would greatly facilitate the development of contactless interactive models, leveraging the widespread availability of moisture.[31,32] Such a system could also eliminate the need for bulky external energy sources.[33–39] Adhyapak *et al.* reported a highly sensitive gold nanowire resistive sensor for humidity and respiration sensing within a relative humidity (RH) range of 11–92%.[40] Wang *et al.* developed a flexible humidity sensor with ultra-fast response for respiratory monitoring and non-contact safety warnings.[41] Korotcenkov *et al.* discussed various sensor types, including capacitive, resistive, impedance-based, and optical fiber sensors. They also analyzed the advantages and limitations of research materials such as carbon nanotubes, graphene, semiconductors, and polymers from an application-oriented perspective.[42] Notably, existing hydroelectric conversion materials convert moisture into electrical signals primarily due to

[a]State Key Laboratory of High-performance Precision Manufacturing, Dalian University of Technology, Dalian 116024, P. R. China. E-mail: yahualiu@dlut.edu.cn
[b]School of Mechanical & Vehicle Engineering, Linyi University, Linyi, Shandong 276000, P. R. China. E-mail: hanhu@lyu.edu.cn
[c]Department of Anaesthesiology, Central Hospital of Dalian University of Technology, Dalian 116033, P. R. China

† Electronic supplementary information (ESI) available. See DOI: https://doi.org/10.1039/d4ra08459d

their abundant dissociable functional groups, *e.g.*, –COOH, –SO_3H, and large specific surface areas, which facilitate moisture absorption and proton ionization.[43–49] However, for applications in portable devices, factors beyond energy conversion efficiency must be considered.

In this study, we report a flexible moisture-electric converter, composed of cellulose nanocrystals (CNCs) and polyvinyl alcohol (PVA). CNCs provide freely mobile H^+ ions, while PVA enhances the flexibility and hydrophilicity of the composite film. Conductive carbon strips serve as electrodes, enabling the film to bend into various shapes without sacrificing power generation performance. This design makes the proposed system highly suitable for wearable devices.

2 Experimental section

2.1 Preparation of the CNC/PVA composite film

CNCs were extracted by hydrolyzing cotton with sulfuric acid, as reported in previous research.[50,51] PVA was procured from Aladdin, and conductive tape was purchased from Taobao (Rigorous). Deionized water, produced using an ultra-pure water machine (Summer-S2-20H, Sichuan Delishi Technology Co., Ltd, China), was used for all experiments. To prepare the composite film, 7 g of PVA was added to 93 g of deionized water and uniformly dispersed using a magnetic stirrer (Fig. 1a). A 5 g CNC suspension (7 wt%) was combined with varying amounts of the PVA suspension (7 wt%), stirred thoroughly for 2 hours, then transferred onto a slide. The material was self-assembled layer by layer at room temperature and dried to form the CNC/PVA composite film. Adjusting the PVA content modified the mechanical properties and structural coloration of the films.

2.2 Fabrication of the non-contact moisture sensor

The CNC/PVA composite film, as the core component of the sensor, absorbs external moisture. Silver (Ag) electrode and conductive carbon strips are adhered to both sides of the composite film to serve as electrodes for signal output. Unlike previous rigid moisture-electric devices with additional metal electrodes,[52] the features of this sensor enhance mechanical flexibility. An external electrochemical workstation (CHI 660E) is connected to the electrodes to capture and visualize electrical signals.

2.3 Characterization

The microstructure is obtained by a field emission scanning electron microscope (FESEM, JSM-7900F Plus, JEOL, Japan). The open-circuit voltage of the sensor is recorded by the electrochemical workstation (ECW, CHI660E, Chenhua, China). Different ambient humidity is controlled by the ambient chamber (DHTHM-50-40-P-ES). The infrared curve is detected by Fourier infrared spectrometer (iN10, Thermo Fisher).

3 Results and discussion

3.1 Characterize of the non-contact moisture sensor

The SEM image of the CNC/PVA composite reveals that the CNCs spontaneously organize into stratified structures, with PVA interspersed among the layers. When the content of PVA is 10%, the cross-sectional morphology (Fig. 1b and c) shows neatly arranged CNC particles with PVA filled the spaces between them. These porous structures provide ample space for moisture adsorption and channels for dissociated ion migration. As the PVA content increases, CNC particles become increasingly coated, causing the loose, layered structure to gradually disappear (Fig. S1†). At PVA content of 20%, 30%, and

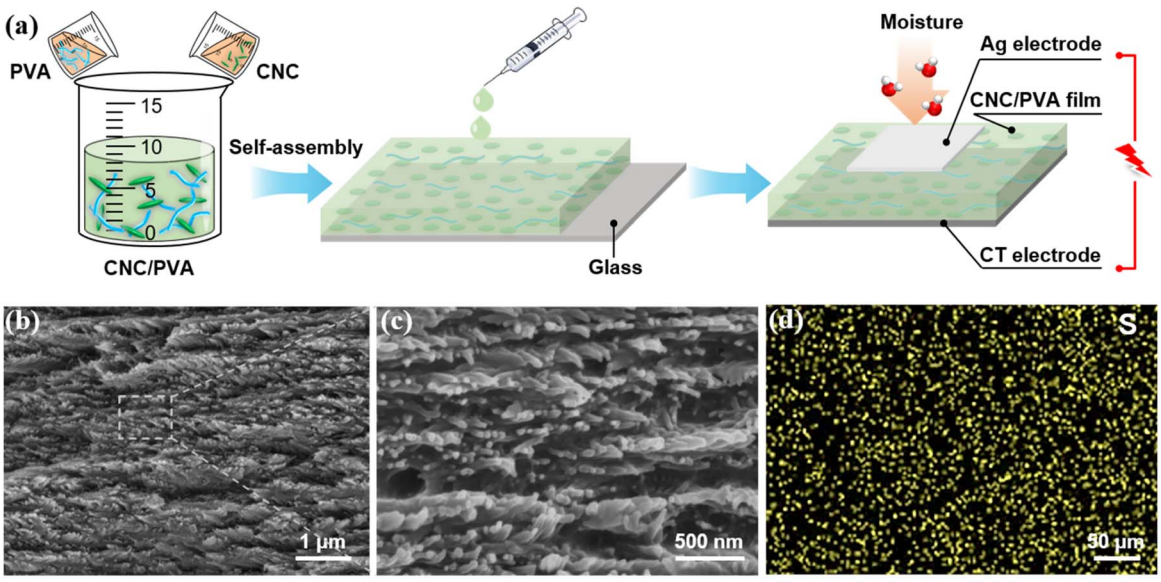

Fig. 1 Preparation of the composite film. (a) Process for preparing the CNC/PVA composite film and fabricating the non-contact moisture sensor. (b and c) SEM image of composite film with content of PVA as 10%. (d) Elemental mapping of S distribution.

40%, the cross-section of the composite progressively smooths, and by about 50%, the layered structure is entirely covered with PVA.

The granular CNCs, derived from sulfuric acid hydrolysis of cotton, are grafted with sulfonic acid groups (–SO_3H) (Fig. 1d), which provided the essential mobile H^+ ions for moisture sensing. EDS analysis confirms a widespread distribution of S elements on the cross section surface of the composite film, indicating the dispersion of H^+ ions. Fourier-transform infrared (FTIR) spectroscopy reveals the chemical composition of CNC, PVA, and their composite films. The characteristic sulfonic acid group peaks in CNC are preserved in the composite, with S=O and S–O stretching vibration observed at 1311.01 cm^{-1} and 1033.94 cm^{-1}, respectively. Additionally, the –OH stretching vibration peak at 3304.17 cm^{-1} indicate the composite's strong hydrophilicity (Fig. S2a†). While both CNC and PVA are hydrophilic, PVA exhibits stronger water absorption, as demonstrated by contact angle measurements (Fig. S2b†). The contact angle of CNC film is 44°, compared to 40° for PVA film, indicating PVA's superior hydrophilicity. This enhanced water absorption underpins the sensor's high sensitivity to moisture stimuli.

3.2 Factors affecting moisture-electrical signal

To achieve high sensitivity in moisture-induced electrical signals, several factors influencing signal generation are explored. As the signal generation area minimally affects output (Fig. S3†), a composite film area of 10 mm × 7 mm was chosen for subsequent experiments to minimize interference. The electrical signals arise from the migration of freely dissociated H^+ ions, which are affected by the composition of the power generation material and its moisture adsorption capacity. The proportion of cellulose nanocrystals (CNC) to polyvinyl alcohol (PVA) significantly affects both the concentration of mobile H^+ ions and the capacity for moisture absorption. CNC, with abundant ionizable functional groups, establishes the ion concentration gradient by dissociating H^+ ions, while PVA enhances the composite film's hygroscopicity due to its higher hydrophilicity compared to CNC. As shown in Fig. 2a, the voltage output rose from 0.4 V to 0.8 V as the PVA/CNC mass ratio reached 50%, driven by improved moisture absorption and ion dissociation. However, increasing the PVA content to 90% reduced the voltage signal to ~0.65 V due to a significant loss of ionizable functional groups, which limited H^+ ion dissociation.

Environmental humidity also significantly impacts signal output. In low-humidity conditions (RH = 20%), the composite film (CNC/PVA = 5 : 5) absorbs less moisture, producing a lower voltage (~0.4 V). Over time, as moisture accumulates within the film, the internal resistance decreases, H^+ migration is enhanced, and the output signal increases. At high humidity (RH = 95%), the signal exceeds 1 V (Fig. 2b and S4†). However, prolonged exposure to high humidity can compromise the stability of the composite, as hydrophilic materials may dissolve. To evaluate the sensor's stability in a humid environment, the CNC/PVA composite film was tested at 95% RH (Fig. 2c). Despite substantial moisture absorption, the film maintained structural integrity and stable signal output for over 100 hours, demonstrating its suitability for long-term use in high-humidity conditions.

3.3 Electric signal generation mechanism of the composite film

To confirm the relationship between moisture and electrical signal generation, a vacuum test was conducted. Initially, at a relative humidity about 60%, the output voltage signal is stable. Upon applying a vacuum, the ambient humidity gradually decreases to 0%, leading the output voltage to drop to 0 V (Fig. 3a). Upon releasing the vacuum, which permitted the re-entry of moisture, the voltage signal swiftly ascends and settle at approximately 0.7 V, thereby validating the signal generation's reliance on the presence of ambient moisture. However, when the composited film was sandwiched between identical-area electrodes in a uniform moisture environment, the symmetrical moisture input produced a negligible voltage signal close to 0 V (Fig. 3b and S5†). This demonstrates that asymmetrical moisture input is essential for generating an electric signal by establishing an effective water gradient. Further experiments confirm the fixed polarity of the sensor's open-circuit voltage. By reversing the connection between the electrochemical workstation and the electrodes, the output signal is observed to invert, thereby confirming the directional nature of ion migration (Fig. 3c).

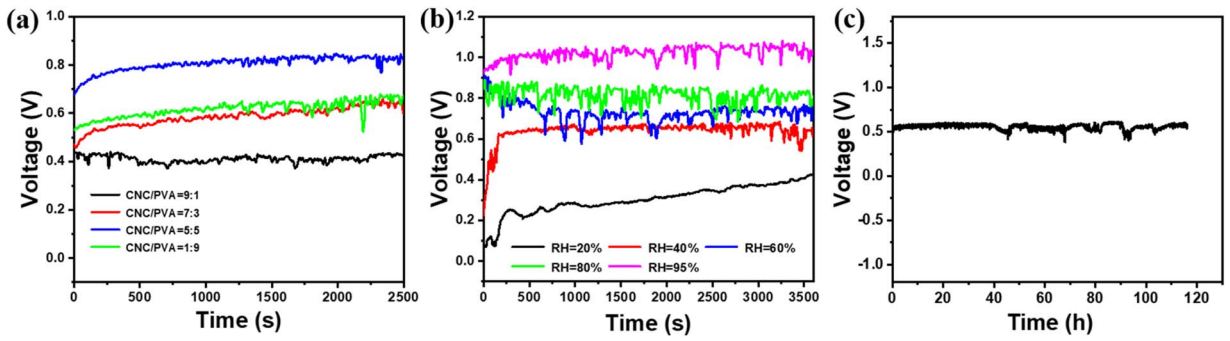

Fig. 2 Electric output of the composite film. Factors influencing the output electrical signal include: (a) the impact of component composition, (b) the effect of ambient humidity, and (c) the stability of the output signal.

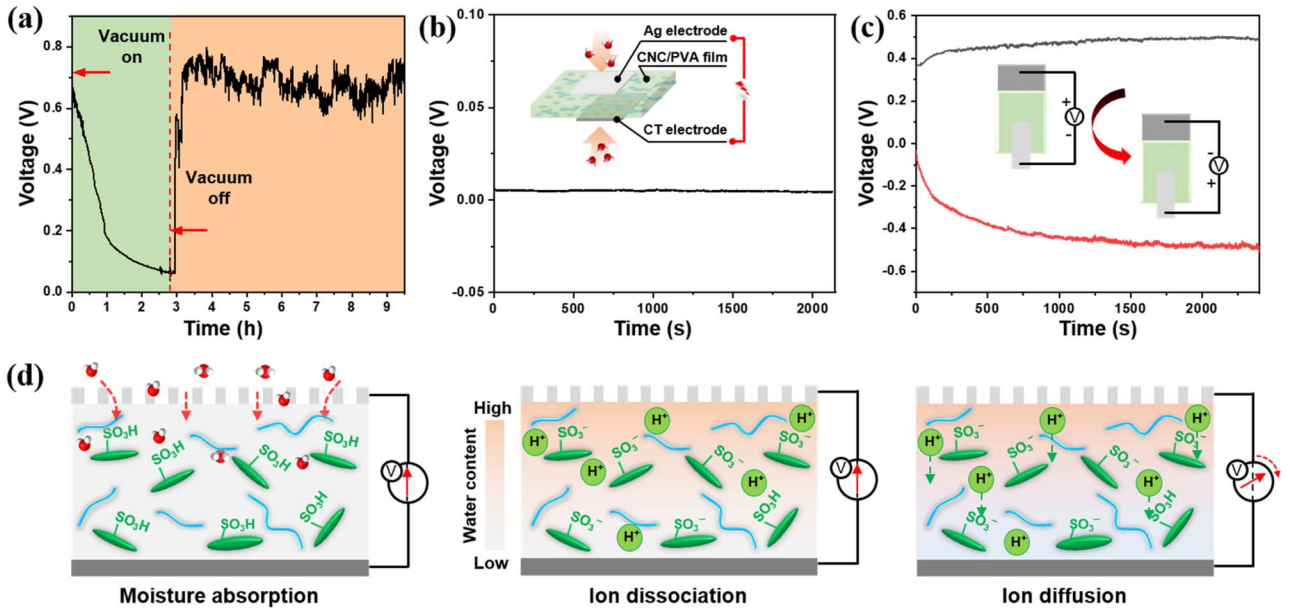

Fig. 3 Mechanism of electrical signal generation. (a) Open-circuit voltage output of the CNC/PVA film. The vacuum is maintained for approximately 3 hours, followed by a vacuum-off period of about 6 hours, corresponding to RH changes from 0% to 60%. (b) Influence of moisture adsorption direction on the electrical signal. (c) Polarity test of the CNC/PVA film. (d) Schematic showing the moisture-to-electric signal conversion principle for the non-contact moisture sensor. Water molecules from a humid environment are adsorbed onto the CNC/PVA film *via* hydrophilic functional groups, which serve as adsorption sites. These functional groups ionize upon moisture absorption, releasing mobile H^+ ions. The directional migration of H^+ ions induces charge separation, resulting in the generation of a voltage signal.

To visualize H^+ diffusion, a CNC/PVA film is placed between two glass tubes containing a methyl orange/ethanol solution. As a pH indicator, methyl orange changes colour from yellow (pH > 4.4) to red (pH < 3.1) in response to dissociated H^+ ions in the solution. When 5 mL water is added to the upper tube, the CNC/PVA film absorbs the water, and its upper surface turns orange and then red, indicating dissociation of H^+ ions. The H^+ ions continue diffusing through the film into the lower tube, changing the solution's colour from orange to red (Fig. S6†). This confirms that rapid H^+ transport, primarily enabled by sulfonic groups ($-SO_3H$) of CNC, drives the electrical signal. Essentially, the signal generation of the non-contact moisture sensor involves three key stages, *i.e.*, moisture absorption, ion dissociation, and charge separation, as shown in Fig. 3d. Specifically, hydrophilic groups (–OH and $-SO_3H$) in the hygroscopic material absorb water firstly. Then the absorbed water dissociates the $-SO_3H$ into mobile H^+ ions and immobilized negatively charged groups ($-SO_3^-$). Finally, the asymmetric moisture absorption creates a concentration gradient in the film, prompting H^+ ions to migrate from high- to low-concentration regions, generating a voltage signal through charge separation.

3.4 Application prospects of the non-contact moisture sensor

The CNC/PVA film converts changes in ambient humidity into electrical signals, and the film is flexible, allowing it to be integrated into wearable devices. For example, embedding the composite film into a mask allows for the monitoring of breathing patterns (Fig. S7 and ESI Movie 1†). Voltage fluctuation curves generated by a slow breathing exhibit broader peaks (Fig. 4a), whereas those produced by rapid breathing display narrower peaks (Fig. 4b), making it suitable for respiratory monitoring in medical applications. As depicted in Fig. 4c, when a finger comes close to the composite film, the moisture from the finger triggers a detectable electrical signal. This signal varies in correlation with the distance of the finger from the

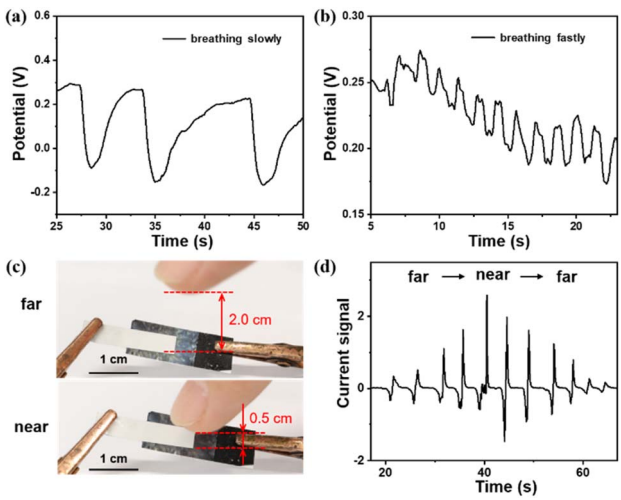

Fig. 4 Application of the non-contact moisture sensor. (a) Electric signal generated by slow breathing. (b) Electrical signal generated by rapid breathing. (c) Schematic showing a finger position indicator. (d) Electrical signals corresponding to varying finger positions.

film, as illustrated in Fig. 4d and further detailed in ESI Movie 2.† These findings indicate the promising potential of integrating this sensor into contactless electronic components, paving the way for gesture-based control systems that respond to the proximity and movement of hands or fingers without the need for physical contact.

4 Conclusions

In summary, we have developed a flexible film functioning as a moisture-electric converter for a non-contact moisture sensor. The intensity of the electrical signal is influenced by the proportion of hygroscopic materials as well as the level of humidity in the surrounding environment. The film demonstrates excellent flexibility, long-term stability, and durability, even in high-humidity environments. By generating distinct electrical signals in response to body humidity, the sensor can capture biological information and enable human-machine information exchange. This work offers valuable insights for advancing non-contact sensor components and establishing human–computer interaction platforms.

Data availability

The data supporting this article have been included as part of the ESI.†

Author contributions

W. G. and Y. L. conceived the project. Y. L. and H. H. supervised the project. W. G., Y. L., and Q. W. designed the project. W. G., Q. W., X. W., and C. L. performed the experiments and analyzed the data. All the authors contributed to manuscript writing and editing.

Conflicts of interest

The authors declare that they have no known competing financial interests or personal relationships that could have appeared to influence the work reported in this paper.

Acknowledgements

We acknowledge the financial support the National Key R&D Program of China (2022YFB4602401), the National Natural Science Foundation of China (52075071, 52105174), the State Key Laboratory of High-performance Precision Manufacturing (ZY202404), and the Fundamental Research Funds for the Central Universities (DUT24YG133).

References

1 Q. M. Wei, W. N. Ge, Z. C. Yuan, S. X. Wang, C. G. Lu, S. L. Feng, L. Zhao and Y. H. Liu, *Nano Res.*, 2023, **16**, 7496–7510.
2 C. X. Shao, J. Gao, T. Xu, B. X. Ji, Y. K. Xiao, C. Gao, Y. Zhao and L. T. Qu, *Nano Energy*, 2018, **53**, 698–705.
3 H. Wang, H. Cheng, Y. Huang, C. Yang, D. Wang, C. Li and L. Qu, *Nano Energy*, 2020, **67**, 104238.
4 X. Wang, Z. Xiong, Z. Liu and T. Zhang, *Adv. Mater.*, 2015, **27**, 1370–1375.
5 J. Feng, L. Peng, C. Wu, X. Sun, S. Hu, C. Lin, J. Dai, J. Yang and Y. Xie, *Adv. Mater.*, 2012, **24**, 1969–1974.
6 E. Cáceres, M. Carrasco and S. Ríos, *Heliyon*, 2018, **4**, e00574.
7 S. An, H. Zhu, C. Guo, B. Fu, C. Song, P. Tao, W. Shang and T. Deng, *Nat. Commun.*, 2022, **13**, 1446.
8 J.-Y. Park, Y. Lee, R. Heo, H.-K. Park, S.-H. Cho, S. H. Cho and Y.-H. Lim, *Sci. Rep.*, 2021, **11**, 23602.
9 Y. J. Choo, G. W. Lee, J. S. Moon and M. C. Chang, *Front. Med.*, 2024, **11**, 1421901.
10 M. B. Khan, M. Rehman, A. Mustafa, R. A. Shah and X. Yang, *Electronics*, 2021, **10**, 1558.
11 J. Wang, W. Lin, Z. Chen, V. O. Nikolaeva, L. O. Alimi and N. M. Khashab, *Nat. Commun.*, 2024, **15**, 1575.
12 A. M. Ashleibta, A. Taha, M. A. Khan, W. Taylor, A. Tahir, A. Zoha, Q. H. Abbasi and M. A. Imran, *Sci. Rep.*, 2021, **11**, 17590.
13 Q. Liang, D. Zhang, T. He, Z. Zhang, Y. Wu, G. Zhang, R. Xie, S. Chen, H. Wang and C. Lee, *Nano Energy*, 2023, **117**, 108903.
14 Y. Dang and M. Cheffena, *IEEE Trans. Antennas Propag.*, 2024, **72**, 7664–7679.
15 L. S. Huang, S. Wang, K. Zhang, Y. X. Li, H. L. Sui, X. F. Bu, Y. Jiang, X. Huang and P. Zhang, *Sens. Actuators, A*, 2023, **360**, 114500.
16 C. Z. Gu, *Sensors*, 2016, **16**, 1169.
17 B. B. Wang, M. Gao, X. F. Fu, M. C. Geng, Y. Liu, N. X. Cheng, J. Li, L. H. Li, Z. J. Zhang and Y. L. Song, *Nano Energy*, 2023, **107**, 108135.
18 S. Li, Y. Shan, J. Chen, X. Chen, Z. Shi, L. Zhao, R. He and Y. Li, *Adv. Mater. Technol.*, 2024, 2401160.
19 S. Das Mahapatra, P. C. Mohapatra, A. I. Aria, G. Christie, Y. K. Mishra, S. Hofmann and V. K. Thakur, *Adv. Sci.*, 2021, **8**(17), 2100864.
20 H. Fayaz, T. Gupta, S. O. Rab, S. K. Jha and S. Kumar, *Drug Discovery Today*, 2024, **29**, 103862.
21 H. L. Zhou, Y. Zhang, Y. Qiu, H. P. Wu, W. Y. Qin, Y. B. Liao, Q. M. Yu and H. Y. Cheng, *Biosens. Bioelectron.*, 2020, **168**, 112569.
22 H. Zhang, Y. Chen, L. Deng, X. Zhu, C. Xu, L. Xie, Q. Yang and H. Zhang, *Nano Energy*, 2024, **132**, 110383.
23 G. Xu, X. Li, X. Xia, J. Fu, W. Ding and Y. Zi, *Nano Energy*, 2019, **59**, 154–161.
24 S. N. Alam, A. Ghosh, P. Shrivastava, U. Shukla, K. Garg, A. C. Edara and N. Sahoo, *Nano-Struct. Nano-Objects*, 2023, **34**, 100980.
25 D. W. Kim, J. H. Lee, J. K. Kim and U. Jeong, *NPG Asia Mater.*, 2020, **12**, 6.
26 Z. Shi, Y. Zhang, J. Gu, B. Liu, H. Fu, H. Liang and J. Ji, *Sensors*, 2024, **24**, 4298.
27 W. Peng and S. Du, *IEEE TCAS-I*, 2023, **70**, 3049–3062.
28 S. X. Wang, X. Wang, C. G. Lu, W. N. Ge, Q. M. Wei and Y. H. Liu, *J. Bionic Eng.*, 2024, **21**, 2340–2348.

29 J. Tan, S. Fang, Z. Zhang, J. Yin, L. Li, X. Wang and W. Guo, *Nat. Commun.*, 2022, **13**, 3643.
30 Y. Y. Lu, G. Yang, Y. J. Shen, H. Y. Yang and K. C. Xu, *Nano-Micro Lett.*, 2022, **14**, 150.
31 J. Tan, X. Wang, W. C. Chu, S. M. Fang, C. X. Zheng, M. M. Xue, X. F. Wang, T. Hu and W. L. Guo, *Adv. Mater.*, 2024, **36**, 2211165.
32 H. Liu, J. X. Qin, X. G. Yang, C. F. Lv, W. T. Huang, F. K. Li, C. Zhang, Y. R. Wu, L. Dong and C. X. Shan, *Nano Res.*, 2023, **16**, 10279–10286.
33 C. Buonocore, R. De Vecchi, V. Scalco and R. Lamberts, *Build. Environ.*, 2018, **146**, 98–106.
34 M. Lee, C.-Y. Chen, S. Wang, S. N. Cha, Y. J. Park, J. M. Kim, L.-J. Chou and Z. L. Wang, *Adv. Mater.*, 2012, **24**, 1759–1764.
35 F. R. Fan, W. Tang and Z. L. Wang, *Adv. Mater.*, 2016, **28**, 4283–4305.
36 F. R. Fan, Z. Q. Tian and Z. Lin Wang, *Nano Energy*, 2012, **1**, 328–334.
37 C. J. Hu, Y. H. Lin, C. W. Tang, M. Y. Tsai, W. K. Hsu and H. F. Kuo, *Adv. Mater.*, 2011, **23**, 2941–2945.
38 S. Bauer, S. Bauer-Gogonea, I. Graz, M. Kaltenbrunner, C. Keplinger and R. Schwödiauer, *Adv. Mater.*, 2014, **26**, 149–162.
39 Y. H. Liu, B. Z. Xiao, Q. M. Wei, Z. C. Yuan, W. Z. Song, L. Zhou and W. N. Ge, *RSC Adv.*, 2024, **14**, 18832–18837.
40 P. V. Adhyapak, A. M. Kasabe, A. D. Bang, J. Ambekar and S. K. Kulkarni, *RSC Adv.*, 2021, **12**, 1157–1164.
41 X. Wang, Y. Deng, X. Chen, P. Jiang, Y. K. Cheung and H. Yu, *Microsyst. Nanoeng.*, 2021, **7**, 99.
42 G. Korotcenkov, N. P. Simonenko, E. P. Simonenko, V. V. Sysoev and V. Brinzari, *Nanomaterials*, 2023, **13**, 1381.
43 L. H. Li, Z. G. Chen, M. M. Hao, S. Q. Wang, F. Q. Sun, Z. G. Zhao and T. Zhang, *Nano Lett.*, 2019, **19**, 5544–5552.
44 J. He, P. Xiao, J. W. Shi, Y. Liang, W. Lu, Y. S. Chen, W. Q. Wang, P. Théato, S. W. Kuo and T. Chen, *Chem. Mater.*, 2018, **30**, 4343–4354.
45 S. Borini, R. White, D. Wei, M. Astley, S. Haque, E. Spigone, N. Harris, J. Kivioja and T. Ryhänen, *ACS Nano*, 2013, **7**, 11166–11173.
46 F. Zhao, H. Cheng, Z. Zhang, L. Jiang and L. Qu, *Adv. Mater.*, 2015, **27**, 4351–4357.
47 H. Cheng, Y. Huang, G. Shi, L. Jiang and L. Qu, Accounts Chem. Res, *Acc. Chem. Res.*, 2017, **50**, 1663–1671.
48 H. Cheng, F. Zhao, J. Xue, G. Shi, L. Jiang and L. Qu, *ACS Nano*, 2016, **10**, 9529–9535.
49 C. Zhang, H. M. Chen, X. H. Ding, F. Lorestani, C. L. Huang, B. W. Zhang, B. Zheng, J. Wang, H. Y. Cheng and Y. Xu, *Appl. Phys. Rev.*, 2022, **9**, 011413.
50 W. N. Ge, Q. M. Wei, F. S. Zhang, Z. X. Feng, X. G. Bai, S. L. Feng, G. Y. Qing and Y. H. Liu, *Cellulose*, 2022, **29**, 4097–4107.
51 W. N. Ge, F. S. Zhang, D. D. Wang, Q. M. Wei, Q. Y. Li, Z. X. Feng, S. L. Feng, X. Y. Xue, G. Y. Qing and Y. H. Liu, *Small*, 2022, **18**, 2107105.
52 J. Xue, F. Zhao, C. Hu, Y. Zhao, H. Luo, L. Dai and L. Qu, *Adv. Funct. Mater.*, 2016, **26**, 8784–8792.